Experimental Thermal and Fluid Science 34 (2010) 81–92

Contents lists available at ScienceDirect

Experimental Thermal and Fluid Science

journal homepage: www.elsevier.com/locate/etfs

Saturated critical heat flux in a multi-microchannel heat sink fed by a split flow system

A.W. Mauro [a], J.R. Thome [b,*], D. Toto [a], G.P. Vanoli [c]

[a] Department of Energetics, Applied Thermofluidynamics and Air Conditioning Systems, FEDERICO II University, p.le Tecchio 80, 80125 Napoli, Italy
[b] Laboratory of Heat and Mass Transfer (LTCM), Faculty of Engineering (STI), École Polytechnique Fédérale de Lausanne (EPFL), Station 9, Lausanne CH-1015, Switzerland
[c] Engineering Department, Sannio University, Corso Garibaldi 107, Palazzo dell'Aquila Bosco Lucarelli, 82100 Benevento, Italy

ARTICLE INFO

Article history:
Received 16 May 2009
Received in revised form 15 September 2009
Accepted 16 September 2009

Keywords:
R236fa
R134a
R245fal
Split flow
Saturated critical heat flux
Microchannel
Pressure drop

ABSTRACT

An extensive experimental campaign has been carried out for the measurement of saturated critical heat flux in a multi-microchannel copper heat sink. The heat sink was formed by 29 parallel channels that were 199 μm wide and 756 μm deep. In order to increase the critical heat flux and reduce the two-phase pressure drop, a split flow system was implemented with one central inlet at the middle of the channels and two outlets at either end. The base critical heat flux was measured using three HFC Refrigerants (R134a, R236fa and R245fa) for mass fluxes ranging from 250 to 1500 kg/m^2 s, inlet subcoolings from −25 to −5 K and saturation temperatures from 20 to 50 °C. The parametric effects of mass velocity, saturation temperature and inlet subcooling were investigated. The analysis showed that significantly higher CHF was obtainable with the split flow system (one inlet–two outlets) compared to the single inlet–single outlet system, providing also a much lower pressure drop. Notably several existing predictive methods matched the experimental data quite well and quantitatively predicted the benefit of higher CHF of the split flow.

1. Introduction

Currently, the electronic industry is strongly interested in small size cooling elements for removing high heat fluxes from microelectronic devices. The next generation of computer microprocessors may need to dissipate heat fluxes over 350 W/cm^2 while maintaining, at the same time, the base temperature below 85 °C. Critical heat flux (CHF) in flow boiling is an important limit to the design and operation of all such devices in which it is important to extract the maximum amount of heat without risk of physical burn-out.

The basic mechanisms of thermal crisis are different according whether the fluid at the outlet is subcooled ($x_{th} < 0$) or saturated ($x_{th} < 0$). The first case occurs, generally, at very high mass velocities, high inlet subcooling and high diameter-to-length ratios, while the second one occurs under the opposite conditions. In the last 40 years, many researchers have investigated the subcooled critical heat flux, since it is the safety limit in the cooling systems for the nuclear power plants. For example, Hall and Mudawar [1,2] collected an extensive database of more than 30,000 points for subcooled CHF.

Most of the more recent saturated CHF [3–13] studies for flow boiling in micro-scale are summarized in Table 1. The maximum diameter considered here is 3.15 mm [4]. The database includes 771 saturated CHF data points, 480 for water, 114 for refrigerants (R113, R236fa, R134a and R245fa) and 177 for cryogenic fluids (helium and nitrogen). The data refers to single and multi-channel configurations for circular and rectangular shapes. Sources and parameter ranges for the CHF data are also provided in Table 1. In all cases, the saturated CHF increased with the mass velocity; this is consistent with the decrease of critical vapor quality (by energy balance) as shown in Katto and Yokoya [5], Wojtan et al. [11], Qi et al. [12] and Agostini et al. [13].

A lack of subcooling effect on CHF was observed in several studies (Bowers and Mudawar [6], Qu and Mudawar [10], Wojtan et al. [11] and Agostini et al. [13]). The investigations, where this effect was found, observed a nearly linear rise in CHF with increasing liquid subcooling.

As far as the geometric effect is concerned, for most studies, the CHF increased when the channel diameter increased and the channel length decreased under the same mass velocity and inlet temperature, as well described by Wojtan et al. [11]. No effect of saturation pressure was pointed out in some studies because of their limited range of tests.

Besides the thermal goal of achieving a high CHF for a microevaporator cooling element for the new generation of computer chips (and for power electronics, etc.), the energetic goal is to operate with as low of pumping power consumption as possible, and

* Corresponding author. Tel.: +39 81 7682303; fax: +39 81 2390364.
E-mail address: john.thome@epfl.ch (J.R. Thome).

0894-1777/$ - see front matter © 2009 Elsevier Inc. All rights reserved.
doi:10.1016/j.expthermflusci.2009.09.005

Nomenclature

A_h	heating area (m^2)
c_{pl}	mean specific heat of liquid (J/kg K)
D	diameter (m)
D_h	hydraulic diameter of each microchannel (m)
D_{he}	heated hydraulic diameter of each microchannel (m)
DT_{sub}	inlet subcooling temperature (K)
E.B.	percentage of points in the error band (%)
f	Fanning friction factor
G	mass velocity (kg/m^2 s)
H	height (m)
H_{tc}	distance from thermocouple to micro channel bottom wall (m)
h	enthalpy (J/kg)
h_{lv}	latent heat (J/kg)
Δh_{in}	inlet subcooling enthalpy (J/kg)
I	current (A)
K	inlet subcooling parameter
k	thermal conductivity of copper heat sink (W/mK)
L	half of the channel length (m)
L_a	half of the adiabatic channel length (m)
L_h	half of the heated channel length (m)
MAE	mean absolute error (%)
MRE	mean relative error (%)
m	total mass flow rate (kg/s)
n	fin efficiency coefficient
P	pressure (Pa)
P_r	reduced pressure
ΔP	pressure drop (Pa)
Q	heating power (W)
q	heat flux (W/m^2) or (W/cm^2)
q_c	critical heat flux, W/m^2 or W/cm^2
$q_{c,0}$	critical heat flux for zero inlet subcooling (W/cm^2)
Re	Reynolds number (GD/μ)
T	temperature (°C)
u	absolute uncertainty, the same dimension of each measured quantity
V	voltage (V)
We_D	Weber number referred to the diameter ($G^2D/\rho_l\sigma$)
We_L	Weber number referred to the length ($G^2L/\rho_l\sigma$)
W	width (m)
x	vapor quality
z	distance along the flow direction from the middle of the micro-channels (m)

Greek letters

α	heat transfer coefficient (W/m^2 K)
ε	relative uncertainty
η	fin efficiency
μ	dynamic viscosity (Pa s)
ξ	single-phase pressure drop coefficient
ρ	density (kg/$m^{3)}$
σ	surface tension (N/m)
υ	specific volume (m^3/kg)

Subscripts

b	base
ch	channel
ch	in channel inlet
f	fin
h	heater
in	inlet upstream the test section
l	liquid
loss	loss
lv	liquid to vapor or vice versa
N	number of channels
out	outlet downstream the test section
pipe	pipe
sat	saturation
slit	slit
sp	single-phase
th	thermodynamic
tp	two-phase
v	vapor
w	wall

hence minimizing the two-phase pressure drop and fluid flow rate through the element are also of primary importance to achieve the ultimate goal of *green, high performance computing*. Therefore, the primary objectives of the present study were:

(1) to collect the first saturated CHF data for flow boiling in a heat sink containing rectangular micro-channels utilizing a split flow (one inlet–two outlets) that is predicted to achieve these goals;
(2) to investigate on the effects of the most important operating parameters on CHF;
(3) to compare the performance of the new feeding system with the standard feeding system with one outlet in terms of attainable CHF;
(4) to assess the accuracy of the leading CHF prediction methods for split flow operation.

2. Experimental apparatus, test procedures and validation

2.1. Flow loop and test section descriptions

A schematic of the test facility is shown in Fig. 1, located in the LTCM laboratory at the EPFL where the experimental work was carried out. The main components are an oil-free magnetic gear pump, a pre-heater, the test section, a plate heat exchanger and a reservoir. The refrigerant evaporates by Joule heating and then condenses in the plate heat exchanger, the latter working with a glycol–water mixture at −20 °C.

The heat sink, fabricated in copper by electro-erosion and milling machining, is shown in Fig. 2. It has 29 channels of $199 \times 756\ \mu m^2$ ($W_{ch} \times H_{ch}$) with a 500 μm wall thickness between each channel. The micro-channels are 30 mm long in the flow direction. An electric heater, $20 \times 20\ mm^2$ of heating area, A_h, was attached on a Printed Circuit Board (PCB); the PCB then was placed on the bottom of the heat sink with the heater located at the middle. Since the channels were heated only for 20 mm in the flow direction ($2L_h$), an unheated 5 mm long zone (L_a) resulted at the two exits of the micro-channels. Between the heater and the bottom surface of the heat sink, a thermal interface material (a thin layer of indium) was placed. The indium has a thermal conductivity of 86 W/mK at 85 °C. To build a firm support and facilitate the assembly, a metal plate of 700 μm thickness and a PEEK plate with a melting point of 250 °C were bolted together with the PCB and the heat sink.

A stainless steel cover composed by a manifold coupled to a plate was fabricated and placed on the top of the heat sink. The fluid enters in the manifold and then passes vertically through a slit, used to inhibit the phenomenon of flow instabilities and vapor back flow as well explained by Bergles and Kandlikar [14]. The slit

Table 1
Parameter ranges of available saturated CHF data for flow boiling in mini/micro-channels.

References	No. of points	Geometry no. channels orientation	Heated length L_h (mm)	Hydraulic diameter D_h (mm)	Fluid	Saturation temperature T_{sat} (°C)	Inlet sub cooling DT_{sub} (K)	Mass velocity G (kg/m^2 s)	CHF (kW/m^2)
Lowdermilk et al. [3]	321	Circ./1/Vert.	64.8–625	1.29–3.12	Water	205–291	114–266	27.4–34,500	192–41,600
Lazarek and Black [4]	32	Circ./1/Vert.	123, 246	3.15	R113	55.8–98.4	2.94–73.8	232–740	93.1–336
Katto and Yokoya [5]	138	Circ./1/Vert.	25.0–200	1.00	Helium	−268	0.00–1.02	10.5–108	0.0783–3.52
Bowers and Mudawar [6]	23	Circ./17/Horiz. Circ./3 /Horiz.	10.0	0.510 2.54	R113	57.2	20.0	28.3–479	352–1052
Lezzi et al. [7]	87	Circ./1/Horiz.	239–975	1.00	Water	222–291	0–248	776–2738	285–2363
Roach et al. [8]	48	Circ./1/Horiz.	160	1.168, 1.448	Water	143–189	76.4–136	247–1037	860–3698
Sumith et al. [9]	6	Circ./1/Vert.	100	1.45	Water	99.9–110	2.15–12.3	23.5–153	147–715
Qu and Mudawar [10]	18	Rect./21/Horiz.	44.8	0.341 (0.215×0.821)	Water	105–109	45.3–77.2	85.9–368	264–542
Wojtan et al. [11]	34	Circ./1/Horiz.	20–70	0.5, 0.8	R134a R245fa	30, 35	4.4–12	353–1533	115–597
Qi et al. [12]	39	Circ./1/Vert.	250	0.531–1.931	Nitrogen	−189, −176	4.97–18.2	415–2799	87.5–233
Agostini et al. [13]	25	Rect./67/Horiz.	20	0.336 (0.223×0.680)	R236fa	20.3–34.3	0.42–15.3	276–992	219–522

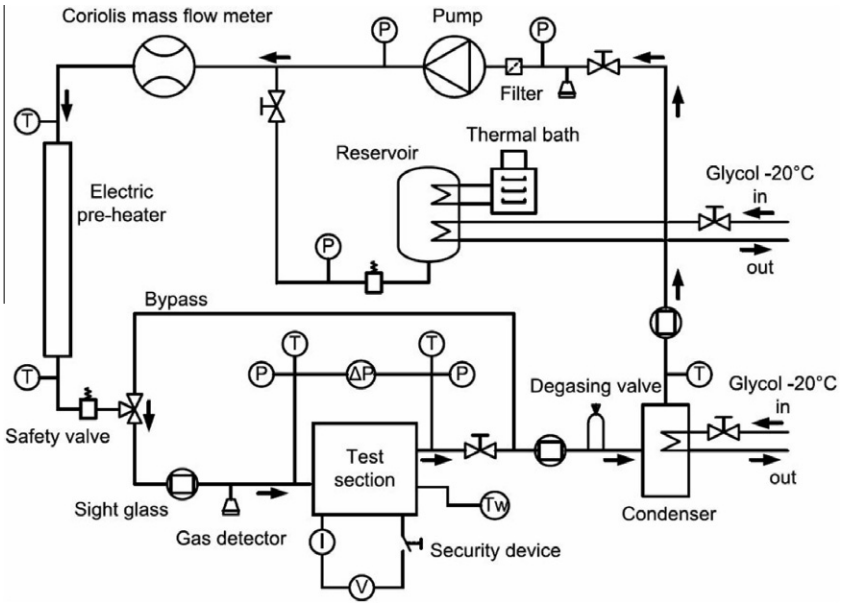

Fig. 1. Schematic diagram of the test facility.

is machined on the back side of the cover plate. The cross-section of the slit and the channels creates a nearly square orifice of $200 \times 199\ \mu m^2$ at the inlet of each channel. After passing through the slit, the flow enters vertically at the middle point of the micro-channels as an impinging flow, then is horizontally split into two flows to the right and left and finally exits at each end of the micro-channels. Therefore, this particular feeding system is formed by one inlet at the middle of the channels and two outlets on the right and left of the channels and is called a split flow system to distinguish it from the standard one with only one inlet and one outlet. A somewhat similar split flow system was tested by Agostini et al. [15] for a silicon test section with both inlet and outlet orifices, but only heat transfer and pressure drop data were obtained, not CHF data. The scheme of the disassembled test section is shown in Fig. 3.

2.2. Measurements, accuracy and data acquisition

The mass flow rate of the refrigerants was directly measured by a Coriolis flow meter, which has an uncertainty of ±0.10% of the reading in the flow range tested for this work. K-type thermocouples, pressure transducers, sight glasses and gas detectors were installed at several locations to monitor changes of parameters inside the loop. The difference between the upstream and downstream pressures of the test section was measured both with two absolute pressure transducers and with a differential pressure transducer. Moreover, the measured upstream pressure was used to calculate the corresponding saturation temperature using REFPROP 8.0. At the same location, the fluid temperature was also measured by a K-type thermocouple with a 500 μm diameter, and subtracting its value from the saturation temperature yielded the inlet subcooling. Downstream of the test section the temperature of the fluid was again measured by a thermocouple.

On the back side of the heat sink, 10 straight grooves were machined perpendicular to the flow direction with their tips equally spaced along the heating length of the middle channel. Then, calibrated K-type thermocouples with a 250 μm diameter were inserted in each groove and fixed by tin soldering to minimize the contact resistance. The top and bottom schematic view of the heat sink and of the arrangement of the thermocouples are shown in

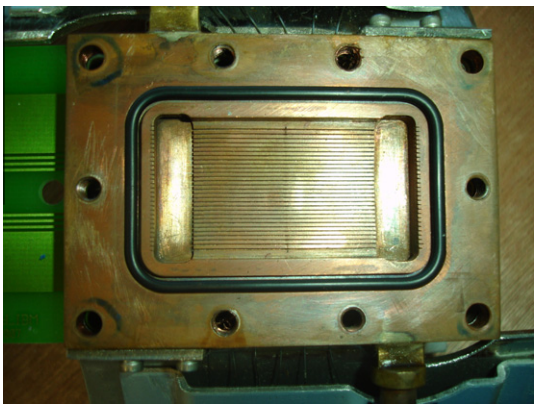

Fig. 2. Photograph of heat sink (199 × 756 μm^2), top view.

Fig. 4. All thermocouples were calibrated before insertion onto the test section by positioning the sensors themselves and two platinum reference probes (accuracy ±0.025 °C as reported by the manufacturer) in a thermally controlled liquid bath; varying the bath's temperature in a range from 5 to 60 °C, with a step of 5 °C. The readings from the thermocouples and the platinum probes were recorded and compared in order to correlate the two sets of data through a least-square fitting. After calibration, the uncertainties for these pressure and temperature measurements were ±10.0 mbar and ±0.1 °C, respectively.

The base heat flux was defined as the ratio between the base heat rate and the heater surface (20 × 20 mm^2). The base heat rate provided by the heater, Q_b, was simply calculated multiplying the voltage, V, by the current, I. From the manufacturer's specifications, the current and voltage measurements had uncertainties equal to 0.09 A and 0.06% of the value, respectively. The uncertainty of the heating area was estimated equal to 5% by taking the standard deviation of repeated measurements.

In this study, the average of 100 data acquired at 5000 Hz was used as a single data point. The average of 60 samples of these points was then recorded as a single experimental point for the boiling curve. Moreover, on these 60 samples the standard deviation was calculated to assess the attainment of steady state. More details about this test facility were presented in an earlier study by Park and Thome [16] on this same test section, but operated with one inlet and one outlet.

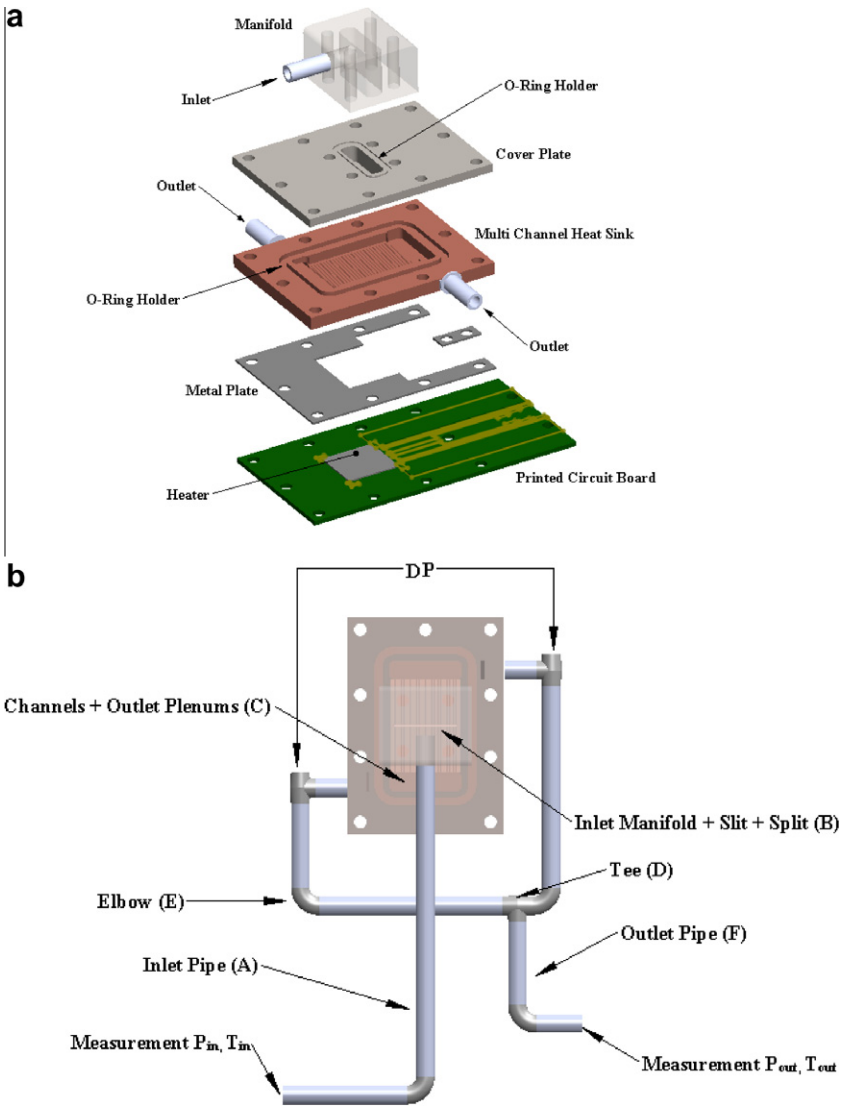

Fig. 3. Schematic diagram of the disassembled test section (a) and upper view of the test section (b).

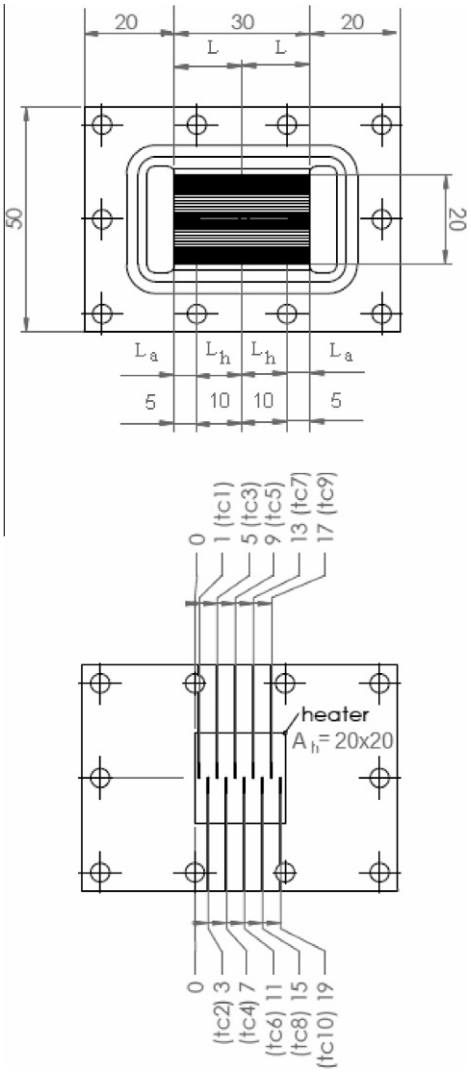

Fig. 4. The schematic view of the heat sink and of the arrangement of the thermocouples.

2.3. Preliminary tests and assumptions

In this work, it was assumed that with the split flow configuration the total mass flow rate circulating into the loop was split in half and, consequently, half of the flow went through one-half of the heated length of the channel (10 mm to each side). For this reason, the mass velocity G was calculated as half of total mass flow rate circulating into the loop, m, divided by the total cross-sectional area of the channels ($N \times W_{ch} \times H_{ch}$), while the heated channel length L_h (10 mm), measured from the centre of heat sink, was assumed as half of the real heated length of the channels ($2L_h$), as depicted in Fig. 4.

Regarding the assumption of an equal split in the flows after the slit, this was indirectly verified with preliminary tests. For all conditions tested, the pressure drop measured between the two outlets was negligible (differential pressure transducer position is showed in Fig. 3). As known, during evaporation, the fact that the pressures at the two outlets, the flow path and the heating power are the same, it is not a sufficient condition to ensure the equal split of the flow. However, during the tests near the crisis, it was verified that the temperature distributions (values) along the middle channels were quite similar. Moreover, since the slit gave a considerable pressure drop, flow instabilities and vapor back flow were inhibited as reported in the work of Agostini et al. [15] Park and Thome [16] with flow visualization. Hence, with this further condition, it was reasonably assumed that the system acts to equalize the mass flow rate to both sides of the split into the micro-channels.

The test section was considered adiabatic to the surroundings. In order to determine the amount of heat provided by the heater that was absorbed by the fluid, the heat loss to the surroundings from the test section was measured with single-phase tests. The ratio between the heat loss to the ambient and the input base heat rate provided by the heater is given as

$$\frac{Q_{loss}}{Q_b} = \frac{VI - mc_{pl}(T_{out} - T_{in})}{VI} \quad (1)$$

where V and I are, respectively, the voltage and the current through the heater, m is the total mass flow rate circulating into the loop, T_{in} and T_{out} are the temperatures measured at the upstream and downstream of the test section and c_{pl} is the mean liquid specific heat. It was found that the heat loss ratio decreased when the base heat flux increased. The tests were run for several mass flow rates with a difference between the fluid at the inlet of the channels and the environment temperatures equal to 20 K. Since the heat loss ratio in single-phase runs attained values that are less than 4% for the highest mass velocity, it was supposed that in evaporation tests with a lower temperature difference with the surroundings, this loss ratio should be even smaller.

Numerical calculations were run to determine which part of the base heating power was transferred to the fluid through the part of the micro-channels corresponding to the heater. A 3D simulation to account for heat transfer by conduction inside the heat sink (with boundary conditions consistent with the test section and the operating conditions tested) showed that at least the 94% of the heating power was transferred to the fluid through the heated part of the micro-channels (with only 5.5% in the ending "adiabatic" zones of the micro-channels and 0.5% in the plenums). This confirmed the appropriateness of using 10 mm as the heated length in evaluating the CHF values.

2.4. Criterion for critical test conditions, test procedure and uncertainties analysis

Before showing CHF results, it is important to describe the criterion used for identifying the CHF conditions and the standard procedure used to determine repeatability in CHF measurements. The fluid always entered the split flow system in subcooled conditions. Even when the fluid was in a single-phase state, several experimental points were recorded after the attainment of steady state in order to build a complete boiling curve as shown in Fig. 5 (using the wall thermocouples closest to the end of the heated zone). As known, the gradient $\Delta q/\Delta T$ increases at the beginning of the two-phase region, while the same gradient tends to decrease approaching the boiling crisis (see Fig. 5). Utilizing this procedure, it was possible to identify the onset of CHF before it actually occurred to ensure the integrity of the test section for multiple tests. In this work, the gradient indicating the onset of CHF was fixed to a value equal to 1 W/K cm^2 for the $\Delta q/\Delta T$ gradient corresponding to the crisis; in preliminary tests above this value, burn-out of the heater occurred and the test section substitution was required.

The propagation of uncertainties for the base heat flux was computed as follows:

$$\varepsilon^2_{q_{c,b}} = \varepsilon^2_{A_h} + \varepsilon^2_V + \varepsilon^2_I \quad (2)$$

where A_h is the heating area of the heater, V and I are the voltage and the current through the heater, respectively.

The maximum uncertainty of the base heat flux was estimated to be equal to ±5.55%. The criterion to determine the critical condition (the $\Delta q/\Delta T$ gradient approach) causes an uncertainty in the determination of the CHF that can be estimated as

$$\varepsilon^2_{\frac{\Delta q_{c,b}}{\Delta T}} = 2 \cdot \left(\varepsilon^2_{q_{c,b}} + \frac{u_T^2}{\Delta T^2} \right) \quad (3)$$

Since the power was increased by a constant step equivalent to an increment of base heat flux in the range 4–10 W/cm^2 near the crisis, for the fixed value of the $\Delta q/\Delta T$ gradient (1 W/K cm^2) and for the tests presented in this paper, the maximum uncertainty encountered in our reported values of CHF was ±10.6%.

3. Experimental results

Table 2 shows the range of operating conditions for the experimental tests carried out to measure the values of saturated base CHF.

3.1. Effect of mass velocity on CHF

With all the fluids tested, the base CHF values increased when the mass velocity was increased but the slope tends to diminish at higher mass velocity as depicted in Fig. 6 for all three fluids. In the experimental results presented here, the annular flow regime is the most probable flow regime according to flow pattern maps. Supposing that the CHF condition occurs in annular flow, we can retain probable that the CHF is associated to a Kelvin–Helmholtz instability phenomenon, since in a previous work by Revellin and Thome [17] their model founded on this assumption (that the trigger for CHF is when the interfacial wave height is equal to the local time-averaged film thickness) returned a good agreement with a large experimental database. Consistent with CHF experimental trends presented in this work, this triggering phenomenon tends to start at lower vapor quality with higher mass velocity because of the thinning of the annular liquid layer by the increased vapor shear.

3.2. Effect of saturation temperature on CHF

In the case of R134a and R236fa, an increase of the saturation temperature always resulted in a slight decrease of base critical heat flux at a constant mass velocity, while R245fa showed a different behaviour with essentially no effect at all, as depicted in Fig. 7. This fact may be related to the influence of the reduced pressure, P_r, on the CHF. As known, the increment of saturation temperature, or reduced pressure, causes an increase in the vapor-to-liquid density ratio, ρ_v/ρ_l, but decreases the latent heat of vaporization, h_{lv}, and the surface tension, σ, as shown in Table 3. As demonstrated from various correlations, the increase of the vapor-to-liquid density ratio should result in an increase of CHF while the decreases of latent heat of vaporization and the surface tension should yield a fall in CHF. These two opposite effects explain why CHF first tends to increase with increasing the reduced pressure and then, after passing by a peak, its value decreases with further increase in the reduced pressure. Probably, in the case of R134a and R236fa, for all tested conditions, the reduced pressure was beyond the value corresponding to the peak of CHF. Instead for R245, the system pressure at tested conditions was less than R134a and R236fa, and it may have been in the range corresponding to the peak of CHF and consequently the CHF was not sensitive to changes in saturation temperatures.

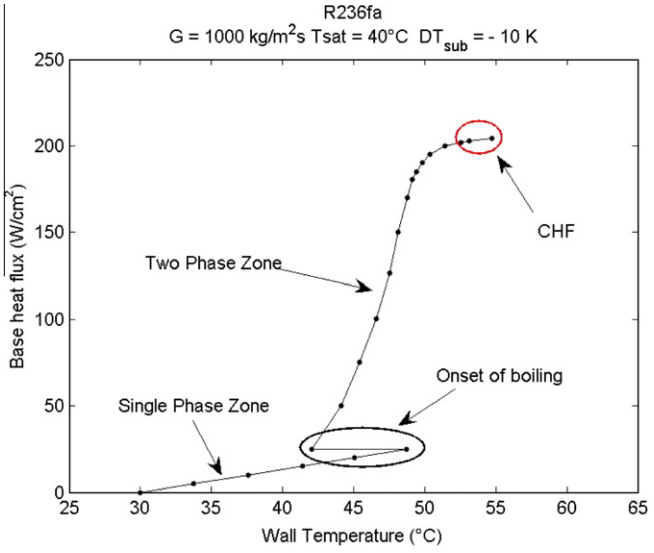

Fig. 5. Boiling curve.

Table 2
Range of operating test conditions for the CHF measurements.

Channel geometry $W_{ch} \times H_{ch}$ (μm^2)	Fluid	Mass velocity G (kg/÷m^2 s)	Inlet subcooling DT_{sub} (K)	Saturation temperature T_{sat} (°C)	No. of points
199 × 756	R134a	500–1500	5–15	20–25	27
	R236fa	500–1000	5–20	30–40	30
	R245fa	250–700	15–25	40–50	20

3.3. Comparison between the split flow system and the single inlet/outlet system: effect of L/D

A selection of the present data have been compared with the previous experimental data measured by Park and Thome [16]. The results reported in Fig. 8a and b showed, respectively, that:

- comparing the systems with the same mass flux in each channel, there is an increase between about 80% and 95% in CHF for R134a while for R236fa and R245fa the increase in CHF also exceeds 80%, due to the fact that the channel heated length for the fluid in the split system is half that in the one inlet–one outlet system;
- comparing the two systems with the same total mass flow rate, there is an increase in CHF and this increase seems to be almost independent of subcooling, but dependent on the fluid. This value is equal to 24% for R134a and 43% for R236fa. No comparable data are available for such a comparison for R245fa.

3.4. Effect of inlet subcooling on CHF

For R236fa and R134a, as shown in Fig. 6, the effect of inlet subcooling on CHF is generally negligible at lower mass velocities, while at higher mass velocities subcooling increases CHF. The positive effect on CHF due to the increase in inlet subcooling might be explained considering that the inlet length before the onset of incipient boiling increases for the same heat flux, mass velocity and saturation pressure and, as a consequence, the corresponding two-phase length is reduced. This fact, as demonstrated by many experimental studies that showed an inverse relationship between saturated CHF and heated length, could cause the increment of CHF. Since the increase of incipient boiling length becomes less significant when the mass velocity decreases, the increment of CHF tends to be negligible. The maximum percentage increment of CHF was recorded for R134a and is equal to 12%. Actually, R245fa shows an opposite behaviour as depicted in Fig. 6, because at higher mass velocity the increase of critical heat flux is almost

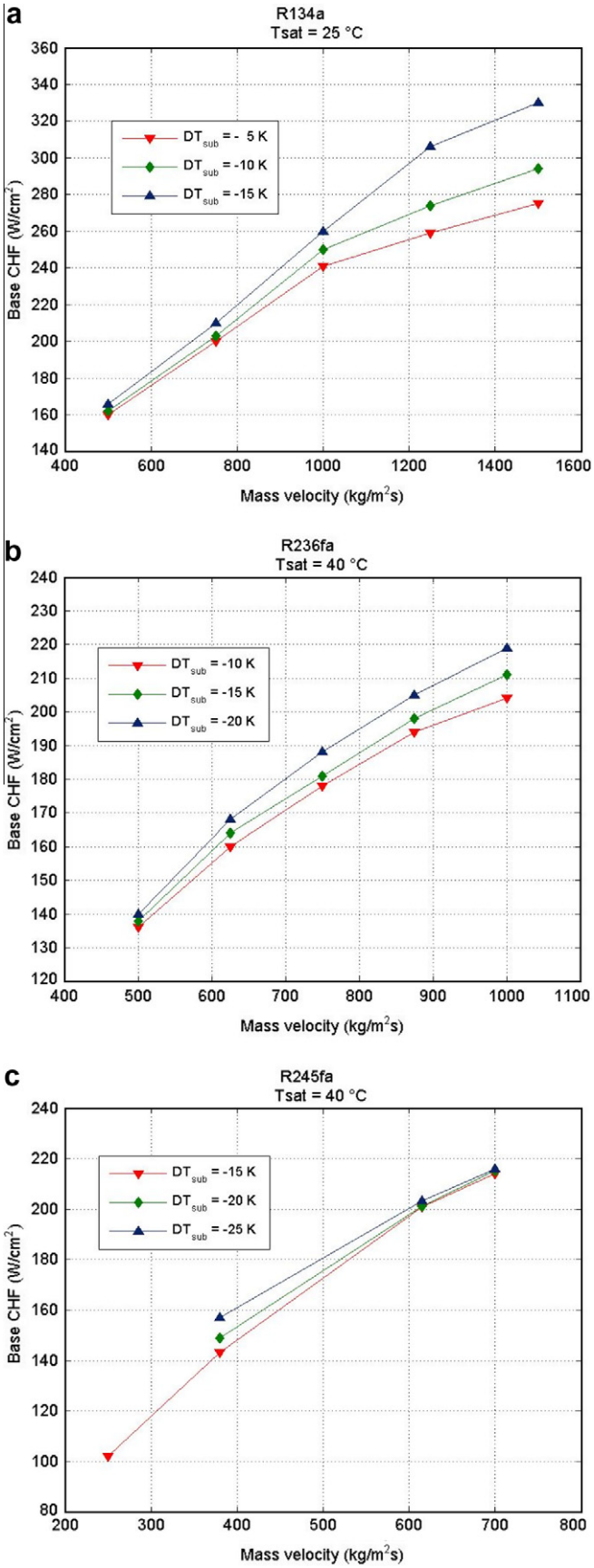

Fig. 6. Effect of mass velocity and inlet subcooling on base CHF for (a) R134a, (b) R236fa, and (c) R245fa.

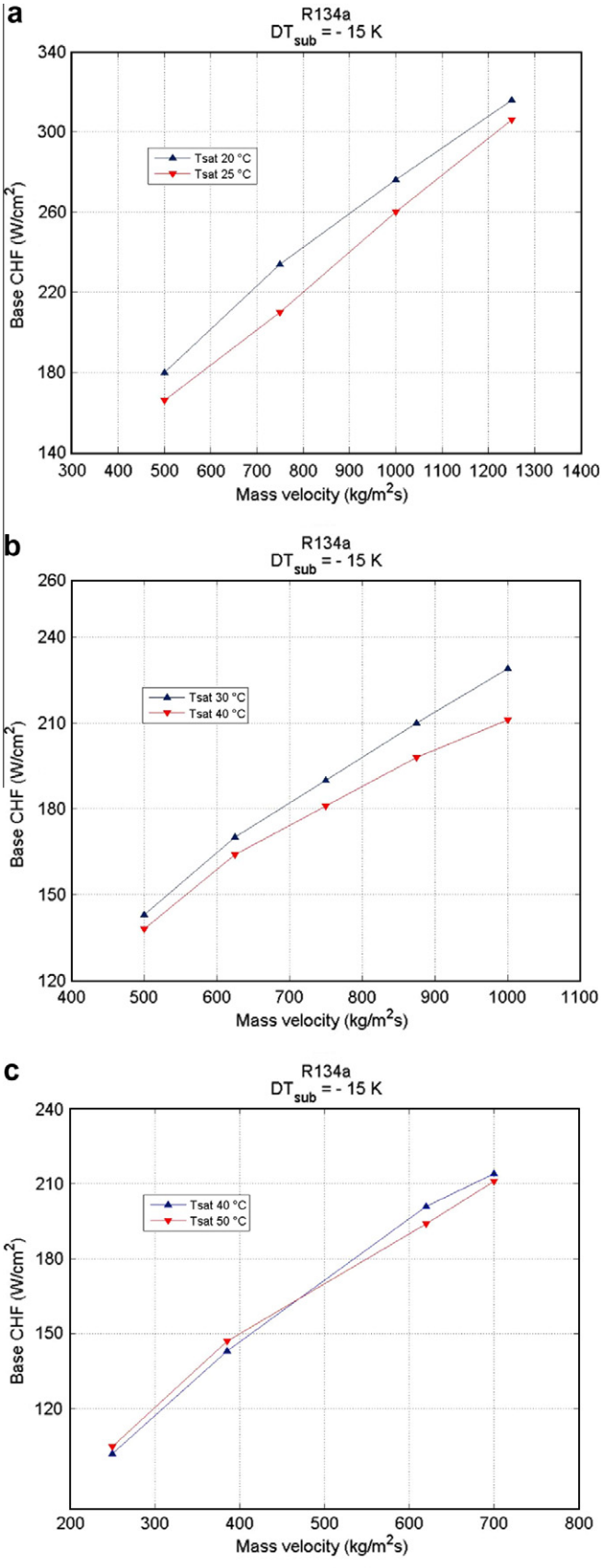

Fig. 7. Effect of saturation pressure on base CHF for (a) R134a, (b) R236fa, and (c) R245fa.

Table 3
Fluid properties varying the reduced pressure.

Fluid	T_{sat} (°C)	P_r (−)	ρ_v/ρ_l (−)	h_{lv} (J/kg)	σ (N/m)
R134a	20	0.141	2.27×10^{-2}	1.8228×10^{5}	8.8×10^{-3}
	25	0.164	2.68×10^{-2}	1.7779×10^{5}	8.1×10^{-3}
Deviation (%)			18.1	−2.5	−7.9
R236fa	30	0.1003	1.61×10^{-2}	1.4295×10^{5}	9.5×10^{-3}
	40	0.1368	2.24×10^{-2}	1.3670×10^{5}	8.3×10^{-3}
Deviation (%)			39.1	−4.4	−12.4
R245fa	40	0.0692	1.08×10^{-2}	1.8174×10^{5}	12.1×10^{-3}
	50	0.0949	1.51×10^{-2}	1.7527×10^{5}	10.9×10^{-3}
Deviation (%)			39.8	−3.6	−9.9

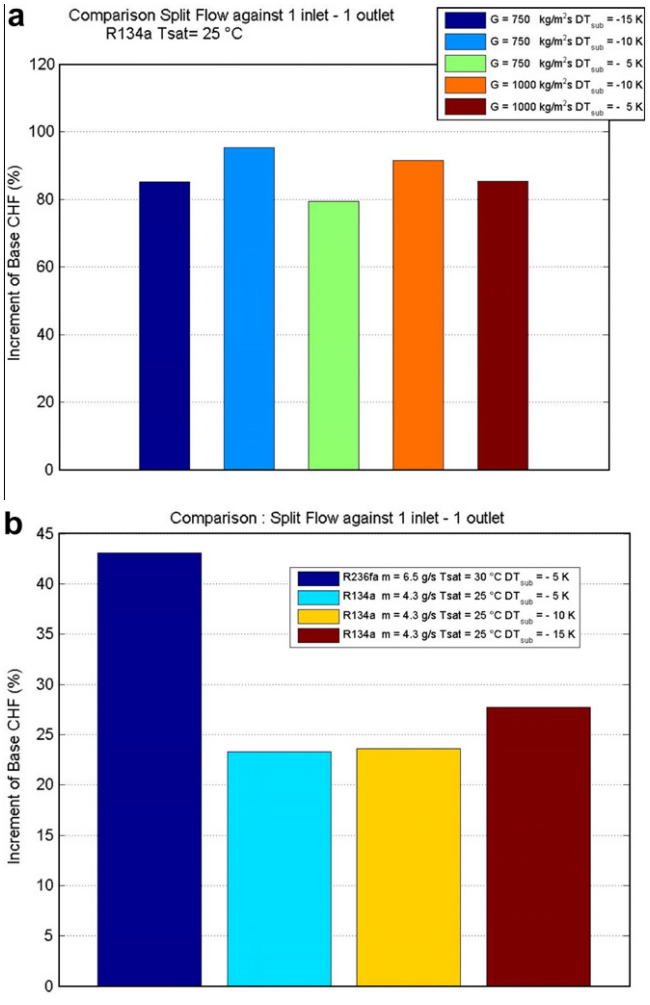

Fig. 8. Increment of base CHF passing from the single outlet system to the split flow system: (a) under the same mass velocity; (b) under the same mass flow rate in the loop.

negligible; however for this fluid the limitations of the test setup did not allow significant variations of the mass flow rate to be tested. In any case, the effect of subcooling is rather minor and thus of secondary importance.

4. Comparison of new results with predictive methods

4.1. Data reduction

CHF prediction methods yield the critical heat flux based on *wall* heat flux, not the *base* heat flux, and hence this requires that the present base CHF values be transformed to wall heat flux values. Thus, in order to compare the experimental results for split flow CHF to the predictive methods available in literature, the experimental data were reduced as described below to obtain the values of CHF based on the effective heat transfer area of the micro-channels accounting for the fin efficiency effect.

4.1.1. Definition of the wall heat flux

Consistent with the assumption that the heat loss to the surroundings were negligible and assuming that the heat transfer trough the fin headers was negligible, the wall heat flux q_w relative to the base heat flux q_b is defined as

$$q_w = q_b \frac{W_{ch} + W_f}{W_{ch} + 2\eta H_f} \tag{4}$$

The fin efficiency η was calculated with the following relations:

$$\eta = \frac{\tanh(nH_f)}{nH_f} \tag{5}$$

$$n^2 = \frac{2\alpha(W_f + L_f)}{k(W_f L_f)} \quad \text{and} \quad n^2 = \frac{2\alpha}{kW_f} \quad \text{if} \quad W_f \ll L_f \tag{6}$$

The heat transfer coefficient α was defined as

$$\alpha(z) = \frac{q_w}{T_w(z) - T(z)} \tag{7}$$

where $T_{sat}(z)$ and $T_w(z)$ are, respectively, the local wall temperature and the local saturation temperature. The wall temperature T_w was calculated from the 1D conduction equation:

$$T_w = T_b - \frac{q_b H_{tc}}{k} \tag{8}$$

where T_b is the base temperature measured by the thermocouple, H_{tc} is the distance between the thermocouple and the inner wall of the channel, and k is the thermal conductivity of the copper heat sink.

4.1.2. Fluid temperature distribution along the channel

The temperature distribution of the fluid along the channel was determined from local pressure and enthalpy distribution, by the integration of the following set of ordinary differential equations:

Momentum equation:

$$\frac{dP}{dz}(z) = G^2\left(2f\frac{v}{D_h} + \frac{dv}{dz}\right) \tag{9}$$

Energy equation:

$$\frac{dh}{dz} = \frac{q}{m/2}W_{ch} \tag{10}$$

In the momentum equation, the friction factor, f, was evaluated by the Fanning relation for the single-phase case; while for the two-phase zone the homogeneous model was used since Ribatski et al. [18] demonstrated that this model was suitable for this purpose. In particular, the relation for the friction factor was the following:

$$f = 0.079\left(\frac{GD_h}{\mu_{tp}}\right)^{-0.25} \tag{11}$$

where the two-phase dynamic viscosity μ was evaluated as

$$\mu_{tp} = x\mu_v + (1 - x)\mu_l \tag{12}$$

In the energy equation q was set equal to the base heat flux for the part of the micro-channels corresponding to the heated zone and equal to zero in the remaining part.

4.1.3. Boundary conditions for pressure and enthalpy distribution inside the micro-channels

To integrate Eqs. (9) and (10) an explicit method was used, fixing the pressure, the enthalpy and the mass flow rate at the inlet of the micro-channels (i.e., at the exit of the slit) as boundary conditions. The mass flow rate was measured directly. The enthalpy was determined supposing that the slit was adiabatic, knowing the pressure and the temperature at the inlet of the system. The pressure, $P_{ch,in}$, was the sum of the measured pressure upstream of the test section, P_{in}, the pressure drop along the section A (inlet pipe) and the pressure drop across section B (inlet manifold + slit + split) as shown in Fig. 3b:

$$P_{ch,in} = P_{in} - (\Delta P_A + \Delta P_B) \tag{13}$$

The fluid state before entering the channels was subcooled. The pressure drop along section A was estimated by implementing a well known single-phase correlation. Hence, in order to calculate the pressure loss in section B, due to the lack of correlation capable of predicting this pressure loss with the desired accuracy, a correlation was fitted to some specifically obtained experimental data for the test section. The procedure implemented to obtain these data is presented below:

(1) From single-phase liquid adiabatic tests, for all the fluids tested, the total pressure drop (P_{in}–P_{out}) was measured for different values of total mass flow rate, m.

(2) The pressure drop relative to all the sections of the test module shown in Fig. 4b, under the same measured values of total mass flow rate, m, were estimated by using the following equations:

(2.1) Pressure drop along the inlet and outlet pipes (sections A–F):

$$\Delta P = \frac{1}{2}\cdot 4 f_{sp}\frac{G_{pipe}^2}{\rho_l}\cdot\frac{L}{D} \tag{14}$$

where

$$f_{sp} = \frac{16}{Re} \quad \text{single-phase Fanning factor – Pouseille – laminar flow if } Re < 2300$$
$$f_{sp} = \frac{0.079}{Re^{0.25}} \quad \text{single-phase Fanning factor – Blasius – turbulent flow if } Re \geqslant 2300 \tag{15}$$

(2.2) Pressure loss due to the bends and the tee (sections D–E)

$$\Delta P = \frac{1}{2}\cdot \xi\frac{G_{pipe}^2}{\rho_l} \tag{16}$$

where ξ depends on the geometry.

(3) From the single-phase adiabatic tests carried out with the standard feeding system (one inlet–one outlet) in a previous investigation by Park and Thome [16] on the same test facility (different test section), the sum of the pressure drop along the channels and the pressure loss into the plenums (section C) was measured, for different values of mass flow rate; these measurements were evaluated by making a regression analysis.

(4) Once a correlation was obtained from the previous fitting procedure, the pressure drop in section C was calculated under the same conditions as the first adiabatic tests and, finally, the pressure loss in section B was obtained from:

$$\Delta P_B = (P_{in} - P_{out}) - (\Delta P_A + \Delta P_C + \Delta P_D + \Delta P_E) \tag{17}$$

By making a *straight-line linear regression*, the pressure loss coefficient, ξ, was found and therefore the dependency of the pressure loss in section B on the mass flow rate and on the density of the fluid:

$$\Delta P_B = \xi\frac{G_{slit}^2}{\rho} \tag{18}$$

The parameter ξ was found to be equal to 8.86.

(5) Thus, it was possible to obtain the local pressure at the beginning of the channels for any desired condition by using Eq. (13).

4.1.4. Calculating procedure

With the momentum and energy equations, fixing the boundary conditions, the pressure and enthalpy distribution were then obtained, checking, during the integration, the phase of the fluid in order to adapt the friction factor used in the momentum equation to be single-phase or two-phase. From the fluid temperature distribution and wall temperature distribution, the heat transfer coefficient, the fin efficiency and the wall heat flux could then all be calculated.

4.1.5. Remarks on this procedure

For the inlet zone where the fluid flow was single-phase, an expression of the friction factor for single-phase flow was used. Hence, any subcooled boiling effect on the pressure drop in the subcooled region was neglected and, at the same time, it was assumed that the evaporation started at the point of the liquid saturation of the bulk fluid enthalpy. Moreover, the relations for pressure drops in the single-phase contraction had an expression that it is strictly valid for single-phase flow: during the tests the large subcooling prevented flashing of the fluid inside the slit. Furthermore, the singular pressure drop of the slit was significantly larger than that of the subcooled zone, making this procedure appropriate.

The procedure described above to reduce the CHF data involves the assumption of an adiabatic top cover plate on top of the fins. Actually, a stainless steel cover plate was clamped onto the top of the copper fins of the heat sink, forming the top side of the flow channels. In earlier tests with a glass cover plate [16], it was observed that only point contacts were made, representing a very large contact resistance that rendered the top plate adiabatic. To account for the uncertainty due to this adiabatic assumption in calculating the wall heat flux, one can estimate the heat loss as if the 756 μm fin was 99.5 μm higher with a thermal conductivity of stainless steel as opposed to copper for this extension, including a small contact resistance. Such a calculation shows that the heat loss of the top stainless steel plate is indeed negligible compared to the stated experimental error noted earlier, especially if a contact resistance is inserted in the analysis.

4.2. Existing predictive methods chosen for the comparison

The first three methods include the effect of subcooling on CHF:

Katto–Ohno: one of the most widely quoted methods for predicting saturated CHF is the Katto and Ohno [19] correlation. In case of no inlet subcooling, Katto and Ohno gave five correlations that are function of the following dimensionless groups:

$$\frac{q_{c,0}}{Gh_{lv}} = f\left(\frac{\rho_l}{\rho_v}, \frac{\sigma\rho_l}{G^2L}, \frac{L}{D}\right) \tag{19}$$

The correlation to use depends on the fluid properties and the channel geometry. The subcooling effect was taken into account with the following linear relation:

$$\frac{q_c}{Gh_{lv}} = q_{c,0}\left(1 + K\frac{\Delta h_{in}}{h_{lv}}\right) \tag{20}$$

To extend the applicability of their correlations to fluids other than water, the authors carried out several experiments with R12 and helium.

Shah: the Shah [20] CHF correlation is based on a large database including 23 fluids (water, cryogenic fluids, chemicals and liquid metals), channel diameters from 0.315 to 37.5 mm and channel lengths from 1.3 to 940 tube diameters. These data were taken from 62 independent works. The correlation is composed of two sub-correlations; the first one is called the upstream condition correlation (UCC), and is a function of the conditions at the channel inlet, such as the subcooling, while the second one is called the local condition correlation (LCC) and is a function of the exit vapor quality.

Zhang et al.: the empirical correlation of Zhang and co-workers [21] was based on a large CHF database for only water over a channel diameter range of 0.33–6.22 mm; the correlation is very simple to use since, unlike those above, it does not have any conditional statement. The Zhang correlation is:

$$\frac{q_c}{Gh_{lv}} = 0.0352\left[We_D + 0.0119\left(\frac{L}{D}\right)^{2.31}\left(\frac{\rho_v}{\rho_l}\right)^{0.361}\right]\left(\frac{L}{D}\right)^{-0.311} \times \left[2.05\left(\frac{\rho_v}{\rho_l}\right)^{0.170} - x_{in}\right] \quad (21)$$

Unlike the previous methods, the methods below did not notice any subcooling effect and thus did not include a subcooling effect:

Bowers–Mudawar: the correlation of Bowers and Mudawar [6] is expressed by the following equation:

$$\frac{q_c}{Gh_{lv}} = 0.16\left[We_L^{-0.19}\left(\frac{L}{D}\right)^{-0.54}\right] \quad (22)$$

Qu–Mudawar: the correlation of Qu and Mudawar [10] is expressed instead by the following equation:

$$\frac{q_c}{Gh_{lv}} = 33.43\left[\left(\frac{\rho_v}{\rho_l}\right)^{1.11} We_L^{-0.21}\left(\frac{L}{D}\right)^{-0.36}\right] \quad (23)$$

Wojtan et al.: the Wojtan et al. [11] correlation is given by the following expression:

$$\frac{q_c}{Gh_{lv}} = 0.437\left[\left(\frac{\rho_v}{\rho_l}\right)^{0.073} We_L^{-0.24}\left(\frac{L}{D}\right)^{-0.72}\right] \quad (24)$$

Revellin–Thome: Revellin and Thome [17] developed a theoretical model for predicting saturated CHF in uniformly heated circular micro-channels. The model is based on the numerical resolution of a system of five nonlinear differential equations; the system combines the momentum equations for the vapor and liquid phase, the energy equations for the vapor and liquid phase and the Young–Laplace equation at the liquid–vapor interface. The authors supposed that the crisis condition in annular flow is triggered when once the interfacial waves attain the same height as the liquid film thickness.

In a recent work [22], these correlations [6,10,11,17,19–21] have been compared with the available CHF data [3–13] summarized in Table 1. It was found that the best overall method was the Zhang et al. correlation [21] that is capable of predicting the 83.3% of the data within an error band of ±30% as shown in Fig. 9 (in a database dominated by values for water). The method of Revellin and Thome [17], instead, is more accurate to predict the CHF data of refrigerants [4,6,11,13] since more than 99% of the data are predicted within an error band of ±30% with a mean absolute error (MAE) equal to 9.8%. A new comprehensive comparison by Revellin et al. [23] again found the same result for a database containing 2996 points from 19 different laboratories for nine different fluids: that the Zhang method was best for water and that the Revellin–Thome method was best for the other eight fluids.

To take into account the heating on only three sides of the present rectangular channels (consistent with the assumption of adiabatic cover plate), the heated hydraulic diameter D_{he} defined as

$$D_{he} = \frac{4W_{ch}H_{ch}}{2H_{ch} + W_{ch}} \quad (25)$$

has been employed as the reference diameter in place of the hydraulic diameter D_h to adapt the prediction methods to multichannel configuration. The actual mass velocity G in the channels is used in the methods. The wall critical heat flux $q_{c,w}$, calculated by Eq. (4), was used in making these comparisons.

4.3. Results of the statistical comparison

The results of the statistical comparisons are shown in Table 4. The best correlations for predicting the present data were the correlations of Katto and Ohno [19] and Wojtan et al. [11] that predict 100% and 98.7% of the data within an error band of ±20%, with MAE's equal to 5.84% and 8.92%, respectively. As in other recent studies, the Qu and Mudawar [10] method did not work well and was excluded here from the statistics. However, the methods [6,11,19,21] and, in particular, the Revellin and Thome method [17] (having been the best one for the single inlet–outlet tests by Park and Thome [16]) worked quite well. Overall, all the methods tended to underestimate the data, except the method by Bowers and Mudawar [6], perhaps due to the 90° turn in the inlet flow condition for a heated length of only 10 mm. For example, in Agostini et al. [15] the split flow heat transfer data were not well predicted by the three-zone flow boiling model of Thome et al. [24], while the single inlet–outlet heat transfer data in Agostini et al. [25,26] were very accurately predicted. Hence, some downstream effect of the inlet normal to the flow is apparently still felt downstream. The mean absolute errors of the CHF methods, however, never exceeded 15% with the exception of the water-based correlation by Zhang et al. [21].

The Wojtan et al. correlation [11] predicts the increment of CHF obtainable with the split flow system equal to be 94% for the first case (same mass flux) with a mean error of about +10%. Similarly, their correlation predicts an improvement of 36% for the second case (same total mass flow rate), which is close to the average of the two experimental values (33.5%). Thus, the split flow solution was found to provide a significant advantage over the traditional one inlet–one outlet configuration. Furthermore, the pressure

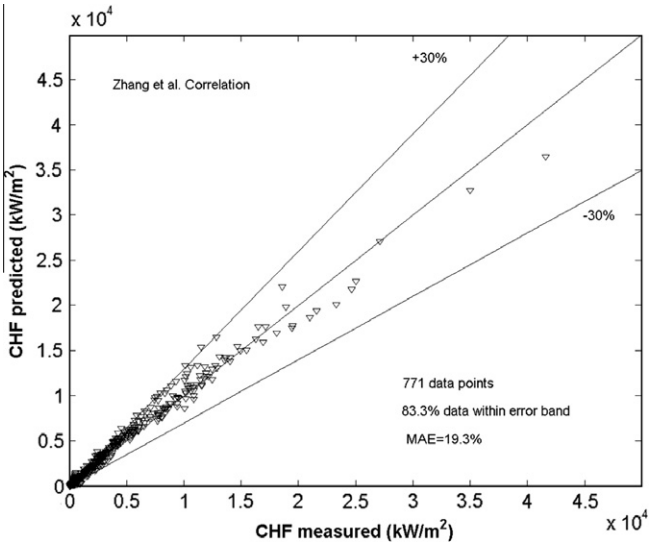

Fig. 9. Saturated CHF data [3–13] predicted by Zhang et al. correlation [21].

Table 4
Results of the statistical comparison among predictive methods.

Methods	Fluids			
	R134a	R236fa	R245fa	All the fluids
Bowers and Mudawar [6]	MAE = 12.6	MAE = 6.51	MAE = 18.0	MAE = 11.6
	MRE = 12.6	MRE = 6.51	MRE = 18.0	MRE = 11.6
	$E.B._{(\pm 30\%)}$ = 100	$E.B._{(\pm 30\%)}$ = 100	$E.B._{(\pm 30\%)}$ = 95.0	$E.B._{(\pm 30\%)}$ = 98.7
	$E.B._{(\pm 20\%)}$ = 100	$E.B._{(\pm 20\%)}$ = 100	$E.B._{(\pm 20\%)}$ = 55.0	$E.B._{(\pm 20\%)}$ = 88.3
Wojtan et al. [11]	MAE = 7.75	MAE = 12.2	MAE = 5.57	MAE = 8.92
	MRE = −7.73	MRE = −12.2	MRE = −0.98	MRE = −7.72
	$E.B._{(\pm 30\%)}$ = 100	$E.B._{(\pm 30\%)}$ = 100	$E.B._{(\pm 30\%)}$ = 100	$E.B._{(\pm 30\%)}$ = 100
	$E.B._{(\pm 20\%)}$ = 100	$E.B._{(\pm 20\%)}$ = 100	$E.B._{(\pm 20\%)}$ = 95.0	$E.B._{(\pm 20\%)}$ = 98.7
Revellin and Thome [17]	MAE = 21.2	MAE = 12.6	MAE = 7.04	MAE = 14.2
	MRE = −19.6	MRE = −9.3	MRE = 3.98	MRE = −9.46
	$E.B._{(\pm 30\%)}$ = 96.3	$E.B._{(\pm 30\%)}$ = 96.7	$E.B._{(\pm 30\%)}$ = 90.0	$E.B._{(\pm 30\%)}$ = 94.8
	$E.B._{(\pm 20\%)}$ = 33.3	$E.B._{(\pm 20\%)}$ = 96.7	$E.B._{(\pm 20\%)}$ = 90.0	$E.B._{(\pm 20\%)}$ = 72.7
Katto and Ohno [19]	MAE = 5.40	MAE = 4.45	MAE = 8.53	MAE = 5.84
	MRE = −2.80	MRE = −3.61	MRE = −0.22	MRE = −2.45
	$E.B._{(\pm 30\%)}$ = 100	$E.B._{(\pm 30\%)}$ = 100	$E.B._{(\pm 30\%)}$ = 100	$E.B._{(\pm 30\%)}$ = 100
	$E.B._{(\pm 20\%)}$ = 100	$E.B._{(\pm 20\%)}$ = 100	$E.B._{(\pm 20\%)}$ = 100	$E.B._{(\pm 20\%)}$ = 100
Zhang et al. [21]	MAE = 23.1	MAE = 26.5	MAE = 21.4	MAE = 24.0
	MRE = −23.1	MRE = −26.5	MRE = −21.4	MRE = −24.0
	$E.B._{(\pm 30\%)}$ = 100	$E.B._{(\pm 30\%)}$ = 96.7	$E.B._{(\pm 30\%)}$ = 100	$E.B._{(\pm 30\%)}$ = 98.7
	$E.B._{(\pm 20\%)}$ = 18.5	$E.B._{(\pm 20\%)}$ = 0.00	$E.B._{(\pm 20\%)}$ = 35.0	$E.B._{(\pm 20\%)}$ = 15.6

drops inside the micro-channels at the same mass flow rate, with the split flow system, were much smaller thanks to the reduction of the mass flux in each microchannel. In conclusion, the split flow system has the benefit of much larger CHF values and reduced pressure drops and further developments in the design of the splitting system could yield to interesting energetic solutions for the cooling of computer chips.

5. Conclusions

New flow boiling saturated CHF data in a multi-microchannel copper heat sink have been collected with three HFC refrigerants: R134a, R236fa and R245fa. The test section was fed by a singular system with one central inlet and two outlets, called split flow, which provided much better performance in terms of CHF attainable compared with the single inlet/outlet system (and also reduced the pressure drop). For all the tests carried out, the saturated CHF increased with mass velocity. For R236fa and R134a, an increase of saturation temperature resulted in a slight decrease of CHF, while the inlet subcooling provided a moderate positive effect on CHF. For R245fa the effect of saturation temperature and inlet subcooling tended to be negligible. The highest CHF values have been reached with R134a (330 W/cm^2 for G = 1500 kg/m^2 s). With this fluid it was possible to achieve higher flow rates with the test facility, thanks to its lower two-phase pressure drop. On the other hand, making the comparison over the same range of mass velocity, R245fa yielded CHF values comparable with R134a. The experimental data were compared with five prediction methods, including one numerical method. The data best matched the correlations of Wojtan et al. [11] and Katto and Ohno [19]. All the methods predicted most of the data within an error band of ±30%. The numerical method of Revellin and Thome [17] also worked quite all, with a MAE and a MRE equal to +14.2% and −9.46%, respectively. The most of the models under-predicted the experimental results, probably due to the effects of the 90° turn in the flow at the start of an only 10 mm long heated length.

References

[1] D. Hall, I. Mudawar, Critical heat flux (CHF) for water flow in tubes – I. Compilation and assessment of world CHF Data, Int. J. Heat Mass Transfer 43 (2000) 2573–2604.

[2] D. Hall, I. Mudawar, Critical heat flux (CHF) for water flow in tubes – II. Subcoolinged CHF correlations, Int. J. Heat Mass Transfer 43 (2000) 2605–2640.

[3] W.H. Lowdermilk, C.D. Lanzo, B.L. Siegel, Investigation of Boiling Burnout and Flow Stability for Water Flowing in Tubes, NACA TN 4382, National Advisory Committee for Aeronautics, Washington, DC, 1958.

[4] G.M. Lazarek, S.H. Black, Evaporative heat transfer, pressure drop and critical heat flux in a small vertical tube with R-113, Int. J. Heat Mass Transfer 25 (1982) 945–960.

[5] Y. Katto, S. Yokoya, Critical heat flux of liquid helium (I) in forced convective boiling, Int. J. Multiphase Flow 10 (1984) 401–413.

[6] M.B. Bowers, I. Mudawar, High flux boiling in low flow rate, low pressure drop mini-channel and micro-channel heat sinks, Int. J. Heat Mass Transfer 37 (1994) 321–332.

[7] A.M. Lezzi, A. Niro, G.P. Beretta, Experimental data on CHF for forced convection water boiling in long horizontal capillary tubes, heat transfer 1994, in: Proceedings of the Tenth International Heat Transfer Conference, vol. 7, Institution of Chemical Engineers, Rugby, United Kingdom, 1994, pp. 491–496.

[8] G.M. Roach Jr., S.I. Abdel-Khalik, S.M. Ghiaasiaan, M.F. Dowling, S.M. Jeter, Low-flow critical heat flux in heated microchannels, Nucl. Sci. Eng. 131 (1999) 411–425.

[9] B. Sumith, F. Kaminaga, K. Matsumura, Saturated flow boiling of water in a vertical small diameter tube, Exp. Therm. Fluid Sci. 27 (2003) 789–801.

[10] W. Qu, I. Mudawar, Measurement and correlation of critical heat flux in two-phase micro-channel heat sinks, Int. J. Heat Mass Transfer 47 (2004) 2045–2059.

[11] L. Wojtan, R. Revellin, J.R. Thome, Investigation of saturated critical heat flux in a single, uniformly heated microchannel, Exp. Therm. Fluid Sci. 30 (2006) 765–774.

[12] S.L. Qi, P. Zhang, R.Z. Wang, L.X. Xu, Flow boiling of liquid nitrogen in micro-tubes: Part II – heat transfer characteristics and critical heat flux, Int. J. Heat Mass Transfer 50 (2007) 5017–5030.

[13] B. Agostini, R. Revellin, J.R. Thome, M. Fabbri, B. Michel, D. Calmi, U. Kloter, High heat flux flow boiling in silicon multi-microchannels: Part III – saturated critical heat flux of R236fa and two-phase pressure drops, Int. J. Heat Mass Transfer 51 (2008) 5426–5442.

[14] A.E. Bergles, S.G. Kandlikar, On the nature of critical heat flux in microchannels, J. Heat Transfer 127 (2005) 101–107.

[15] B. Agostini, J.R. Thome, M. Fabbri, B. Michel, High heat flux two-phase cooling in silicon multi-microchannels, IEEE Trans. Components Packag. Technol. 31 (2008) 691–701.

[16] J.E. Park, J.R. Thome, Critical heat flux in multi-microchannel copper elements with low pressure refrigerants, Int. J. Heat Mass Transfer 53 (2009), doi:j.ijheatmasstransfer.2009.09.

[17] R. Revellin, J.R. Thome, A theoretical model for the prediction of the critical heat flux in heated microchannels, Int. J. Heat Mass Transfer 51 (2008) 1216–1225.

[18] G. Ribatski, L. Wojtan, J. Thome, An analysis of experimental data and prediction methods for two-phase frictional pressure drop and flow boiling heat transfer in microscale channels, Exp. Therm. Fluid Sci. 31 (2006) 1–19.

[19] Y. Katto, H. Ohno, An improved version of the generalized correlation of critical heat flux for the forced convective boiling in uniformly heated vertical tubes, Int. J. Heat Mass Transfer 27 (1984) 1641–1648.

[20] M. Mohammed Shah, Improved general correlation for critical heat flux during upflow in uniformly heated vertical tubes, Int. J. Heat Fluid Flow 8 (1987) 326–335.
[21] W. Zhang, T. Hibiki, K. Mishima, Y. Mi, Correlation of critical heat flux for flow boiling of water in mini-channels, Int. J. Heat Mass Transfer 49 (2006) 1058–1072.
[22] D. Toto, J.R. Thome, R. Mastrullo, G.P. Vanoli, Stato dell'arte delle ricerche sperimentali sul flusso termico critico in condizioni di saturazione in microcanali, in: Proceedings of the XXVI National Heat Transfer Congress UIT, Palermo, 2008.
[23] R. Revellin, K. Mishima, J.R. Thome, Status of prediction of critical heat flux in mini and microchannels, Int. J. Heat Fluid Flow 30 (2009) 983–992.
[24] J.R. Thome, V. Dupont, A.M. Jacobi, Heat transfer model for evaporation in microchannels – Part I: presentation of the model, Int. J. Heat Mass Transfer 47 (2004) 3375–3385.
[25] B. Agostini, J.R. Thome, M. Fabbri, B. Michel, D. Calmi, U. Kloter, High heat flux flow boiling in silicon multi-microchannels – Part I: heat transfer characteristics of refrigerant R236fa, Int. J. Heat Mass Transfer 51 (2008) 5400–5414.
[26] B. Agostini, J.R. Thome, M. Fabbri, B. Michel, D. Calmi, U. Kloter, High heat flux flow boiling in silicon multi-microchannels – Part II: heat transfer characteristics of refrigerant R245fa, Int. J. Heat Mass Transfer 51 (2008) 5415–5425.